Annals of Biomedical Engineering, Vol. 39, No. 5, May 2011 (© 2011) pp. 1403–1413
DOI: 10.1007/s10439-010-0239-4

Effect of Hemodynamic Forces on Platelet Aggregation Geometry

ELHAM TOLOUEI,[1,2] CHRISTOPHER J. BUTLER,[1] ANDREAS FOURAS,[1,2] KRIS RYAN,[1] GREGORY J. SHEARD,[1] and JOSIE CARBERRY[1]

[1]Fluids Laboratory for Aeronautical and Industrial Research (FLAIR), Department of Mechanical and Aerospace Engineering, Monash University, Melbourne, VIC 3800, Australia; and [2]Division of Biological Engineering, Faculty of Engineering, Monash University, Melbourne, VIC 3800, Australia

(*Received 25 November 2010; accepted 23 December 2010; published online 4 January 2011*)

Associate Editor Konstantinos Konstantopoulos oversaw the review of this article.

Abstract—The shear rate dependence of platelet aggregation geometries is investigated using a combination of *in vitro* and numerical experiments. Changes in upstream shear rate, γ_{Pw}, are found to cause systematic changes in mature platelet aggregation geometries. However, γ_{Pw} is not the only factor determining the shear rate experienced by a platelet moving over, and adhering to, a platelet aggregation: flow simulations demonstrate that naturally occurring variations in platelet aggregation geometry cause the local shear rate on the surface of a mature platelet aggregation to vary between zero and up to eight times γ_{Pw}. Additionally, as a platelet aggregation grows, systematic changes in geometry are found, indicating that the local shear field over a growing platelet aggregation will differ from that over mature platelet aggregations.

Keywords—Platelets, Platelet aggregation, Shear rate, Mature platelet aggregation, Exposure time.

INTRODUCTION

The central function of platelets is to arrest bleeding at the site of vascular injury by adhering to the vessel wall and forming a platelet aggregation. However, platelet adhesion and excessive platelet aggregation also play a role in arterial diseases leading to heart attacks and stroke.[1,4,12,13] The biochemistry of platelet function has been extensively studied and myriad mechanisms have been shown to contribute to the adhesion and aggregation of platelets leading to thrombus formation.[13,14] Adhesion of platelets to the vessel wall is initiated when the endothelial cells are damaged or platelets are exposed to thrombogenic elements in the subendothelial matrix. Platelet aggregation is a complex, multistage process that involves many elements, including platelet membrane receptors, plasma proteins, and receptors on the vessel wall.

It has been known for sometime that hemodynamics plays a role in platelet aggregation, and critical platelet functions have been shown to depend on hemodynamic forces.[5,16] Hemodynamic forces in the vasculature are dominated by shearing stresses, which can be characterized by the shear rate. For a simplified flow, the shear rate is given by $\gamma = \mathrm{d}u/\mathrm{d}y$, where u is the flow velocity and y is the direction perpendicular to the flow. Most commonly the reported shear rate $\gamma_{Pw} = \mathrm{d}u/\mathrm{d}y|_{y=0}$ is the wall shear rate calculated by assuming a Poiseuille flow. Unless stated otherwise, the shear rate quoted from previous studies is the estimated wall shear rate γ_{Pw}.

The shear rate dependence of platelet function can be loosely characterized by considering three shear regimes: low shear rate ($<1000\ s^{-1}$), high shear rate (1000–10,000 s^{-1}), and very high (pathological) shear rate ($>10{,}000\ s^{-1}$).[7] The pathways of platelet adhesion are shear rate dependent: at low shear rates adhesion is to collagen, via $\alpha_2\beta_1$ or GPVI, and immobilized vWF via integrin $\alpha_{IIb}\beta_3$. At higher shear rates platelet adhesion is primarily onto vWF with initial recruitment via GPIb and stabilizing recruitment requiring the activation of integrin $\alpha_{IIb}\beta_3$. At pathological shear rates, found in stenosed vessels, adhesion and aggregation occur independently of integrin $\alpha_{IIb}\beta_3$ and activation.[5] Recruitment and aggregation of additional platelets into the growing platelet aggregations involves many of the mechanisms of platelet adhesion. Thus the hemodynamic considerations of platelet adhesion are also relevant to subsequent aggregation.[15]

Address correspondence to Josie Carberry, Fluids Laboratory for Aeronautical and Industrial Research (FLAIR), Department of Mechanical and Aerospace Engineering, Monash University, Melbourne, VIC 3800, Australia. Electronic mail: josie.carberry@monash.edu

Recently platelet aggregation was also found to depend not only on the magnitude of the upstream shear rate but also on the time history of the shear rate on an individual platelet.[8] At high upstream shear rates, platelets preferentially adhere in low-shear zones found near the downstream surface of a platelet aggregation. Platelets adhering in these locations experience a peak shear rate, followed a short time later by low shear rate. This adhesion is predominantly via activated integrin $\alpha_{IIb}\beta_3$. The adhesion that does occur in the peak shear rate zone is predominantly via GPIb. The dependence on time varying shear rate has important implications for understanding how a platelet aggregation grows and also under what conditions platelet aggregation growth ceases. The shear rate experienced by a platelet is not governed purely by the upstream shear rate but also by the local shear rate, found around a platelet aggregation. The geometry of a platelet aggregation is determined by the adhesion of its constituent platelets. However, the platelet aggregation geometry, coupled with the upstream shear rate determines the local shear rate in which adhesion occurs and thus it is clear that the process by which the final platelet aggregation geometry is formed is complex. In this paper we investigate the shear rate dependence of platelet aggregation geometries at upstream shear rates between 1200 and 1800 s^{-1}. Additionally, by numerically calculating the flows over platelet aggregations developed in the *in vitro* model we are able to report the distribution of local shear rate, γ_{Local} around a platelet aggregation.

MATERIALS AND METHODS

Platelet Aggregation Preparation

Platelet aggregations were allowed to develop under controlled flow conditions inside a glass microchannel; they were then fixed and scanned to measure their geometry. The method used to generate the platelet aggregations is described briefly below, for further details see Refs. 6, 8, 9. Figure 1a is a schematic of the experimental setup used to prepare the platelet aggregations. Glass microchannels with cross-section 2 × 0.2 mm (width × height) and length 100 mm were coated with collagen type I (10 μg/mL) to promote platelet adhesion. Whole blood, obtained from healthy human donors and anticoagulated with Hirudin, was perfused through the coated microchannels using a PHD 22/2000 programmable syringe pump (Harvard Apparatus, MA, USA) to enable interaction of platelets with the coated matrix. All experiments were conducted with the approval of the Monash University Standing Committee on Ethics in Research Involving Humans. Hirudin is a potent natural inhibitor of thrombin and is well suited to the study of platelet behavior as it does not alter platelet recruitment, only affecting the final stages of coagulation. Blood was taken from healthy donor with pH 7.35–7.45 and maintained at 37 °C using a waterbath. During the experiments the blood was exposed to room temperature (approx. 21 °C) for less than 12 min. The short experimental time would cause only minor changes in blood temperature and pH. Platelet aggregation was monitored using a DM IRB epi-fluorescent inverted microscope (Leica Microsystems, Germany) equipped with a camera for video recording and online checking. The upstream shear rate quoted for each experiment is the wall shear rate calculated assuming a laminar Poiseuille channel flow:

$$\gamma_{Pw} = 6Q/wh^2 \quad (1)$$

where Q is the flow rate, w and h are the channel width and height, respectively.

This is the estimated shear rate at the channel wall without flow modification due to the presence of platelet aggregations. At a given upstream shear rate, the collagen matrix was exposed to blood for a controlled period described as the exposure time. Once the specified exposure time for the experiment had passed, blood flow was stopped and the platelet aggregations fixed using paraformaldehyde solution.

Syringe Pump Flow Loop

The experiments were performed using a 50 mL glass syringe in a Harvard programmable syringe pump: an apparently well-established flow generation method. However, when a flow probe (TS410 transit-time tubing flowmeter with a 1PXN flow probe, Transonic Systems Inc., NY, USA) was installed 50 mm from the syringe pump, the nominally constant flow from the pump was found to be highly pulsatile, as shown in Fig. 1b. It was determined that the flow pulsatility was a direct function of the rotational velocity of the pump screw mechanism and was therefore a function of both the flow rate and the syringe diameter. Whilst changing the syringe diameter and flow rate had an effect on the magnitude of the flow pulsatility, as did changing the flow direction from pushing to pulling, with only a short length of tubing (100 mm ID 0.063″) significant flow pulsatility was always present.

To obtain repeatable steady flow in the microchannels a long inflow length (690 mm) of larger-diameter tubing (tygon tube, ID 0.25″) followed by a shorter section (70 mm) of smaller-diameter tubing (silicon tube, ID 0.063″) was placed between the pump and the microchannel to damp out oscillations. Flow measurements both upstream and downstream of the

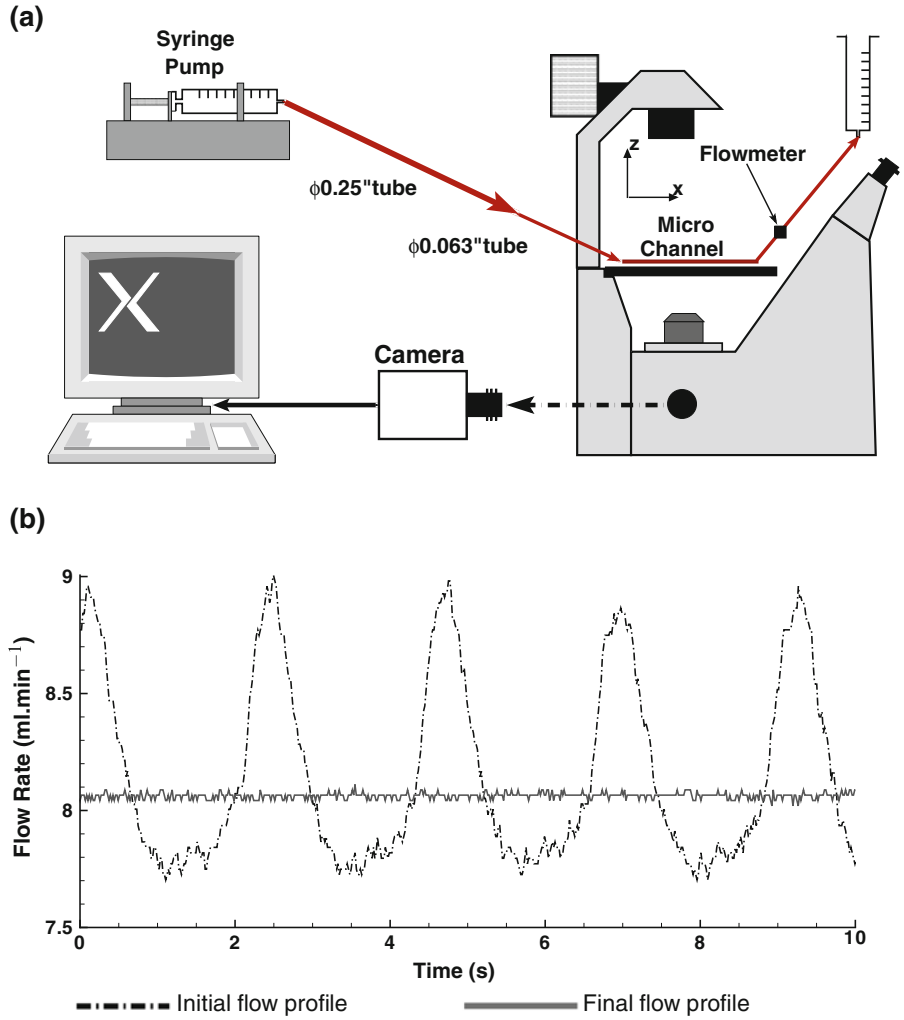

FIGURE 1. (a) Schematic showing the experimental setup for preparing fixed platelet aggregations. (b) Flow rate profiles immediately downstream of the microchannel. *The dashed line* shows an unacceptably pulsatile flow in the initial setup using only 100 mm of ID 0.063″ inflow tubing. *The solid gray line* shows the flow profile for the final experimental setup using 690 mm of ID 0.025″ tubing followed by 70 mm of ID 0.063″ tubing to damping the pulses to an insignificant level.

microchannel demonstrated constant flow (Fig. 1b) for all flow rates used in the experiments. The Re based on the channel height is 2.42, 3.21, and 3.63 at shear rates of 1200, 1600, and 1800 s^{-1}, respectively.

Measurement of Platelet Aggregation Geometry

The geometry of the prepared fixed platelet aggregations was measured using an in-house high spatial resolution bright field scanning microscopy technique. The glass microchannel with fixed platelet aggregations was placed horizontally on a microscope equipped with a 0.1 μm resolution vertical sample stage. While the focal plane was kept fixed, the sample was traversed allowing scanning of the complete aggregation geometry through the measurement plane. The stage is pre-calibrated and certified to have a precision of 0.1 μm. The stage accuracy was thoroughly tested utilizing the method described in Fouras *et al.*[2] Images were recorded through a 2.5× adapter to allow full utilization of the camera sensor (MotionPro X3, Redlake Inc., USA). The whole microchannel was mapped at low resolution (×5 dry objective, NA 0.15), as shown in Fig. 2a, to estimate platelet aggregation locations inside the microchannel. Selected platelet aggregations (not immediately adjacent to the microchannel wall) were imaged at high resolution (×40 dry objective, NA 0.5) with a vertical scanning step of 1 μm to produce a stack of images for three-dimensional reconstruction. The images were analyzed using an edge detection algorithm to identify the edge of the platelet aggregations in each z-plane allowing the combination to form complete platelet aggregation surfaces. A sample high-resolution platelet aggregation

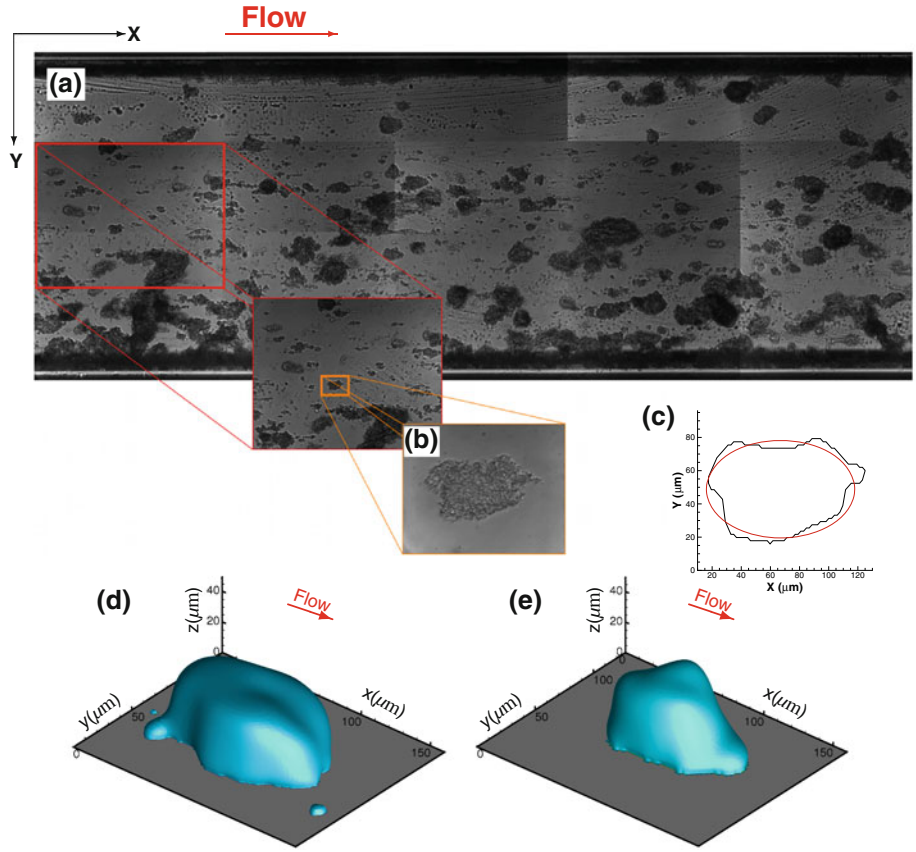

FIGURE 2. Measurement of platelet aggregation geometries using bright field scanning microscopy and image reconstruction. (a) The channel was first mapped at low resolution (×5 objective) to determine the location of individual platelet aggregations. (b) Individual platelet aggregations were imaged at high resolution (×40 objective) at vertical increments of 1 μm. (c) Typical fitting of an ellipse to the platelet aggregation. (d, e) The image stacks were reconstructed into individual three-dimensional platelet aggregation geometries.

image slice is shown in Fig. 2b and selected three dimensional reconstructed platelet aggregation geometries in Figs. 2d and 2e).

A number of geometric parameters were developed to characterize the platelet aggregations. The platelet aggregation centroid height, z_c, is defined as the weighted-average location of all mass points within the platelet aggregation.

$$z_c = \frac{\sum_{i=1}^{k} v_i z_c}{\sum_{i=1}^{k} v_i} \tag{2}$$

It is also useful to characterize the platelet aggregations at each z level. The in-plane centroid (x_c, y_c) is the location of the centroid at a given z level and allows us to identify how the shape of the platelet aggregations varies with height.

$$x_c(z) = \frac{\sum_{i=1}^{m} A_i x_c}{\sum_{i=1}^{m} A_i} \tag{3a}$$

$$y_c(z) = \frac{\sum_{i=1}^{m} A_i y_c}{\sum_{i=1}^{m} A_i} \tag{3b}$$

To study the evolution of platelet aggregation geometry, a method to calculate an average platelet aggregation geometry was developed. Each platelet aggregation was analyzed at $n = 100$ equi-spaced z levels using a least squares method to fit an ellipse to the cross-sectional profile. A typical fitted ellipse is shown in Fig. 2c. The major and minor axes of the fitted ellipse at each z level were averaged across all z levels yielding a_{ave} and b_{ave}, respectively. In all cases the major axis was aligned closely with the upstream flow with the average inclined angle of 3.96° ± 1.36°, 2.99° ± 0.77°, and 4.99° ± 1.29° ($p = 0.1$) at upstream shear rates 1200, 1600, and 1800 s^{-1}, respectively. To compare the averaged profile of the platelet aggregations, the major and minor axes were normalized with the maximum platelet aggregation height, h_{max}

$$a^*_{ave}(z) = \frac{1}{n}\sum_{i=1}^{n} \frac{a_i}{h_{max,i}} \tag{4a}$$

$$b^*_{ave}(z) = \frac{1}{n}\sum_{i=1}^{n} \frac{b_i}{h_{max,i}} \tag{4b}$$

To allow comparison between platelet aggregations a normalized in-plane centroid was developed which compares the location of the in-plane centroid at each z level with the position of the in-plane centroid at the platelet aggregation base ($z = 0.0$). The displacement is then normalized by the major or minor axes of an ellipse fitted to the base level of the platelet aggregations:

$$x_c^*(z_i) = \frac{x_c(z_i) - x_c(z=0)}{a(z=0)} \tag{5a}$$

$$y_c^*(z_i) = \frac{y_c(z_i) - y_c(z=0)}{b(z=0)} \tag{5b}$$

If the platelet aggregation shape is such that each level is centered directly above the base centroid then both x_c^* and y_c^* will be zero at each z level. If the platelet aggregation geometries above the base level is weighted downstream or upstream then the values of x_c^* will become positive or negative, respectively.

Numerical Simulations

At $\gamma_{Pw} = 1800\ s^{-1}$, platelet aggregations close to the statistical median shape were selected for numerical analysis of flow. In each case the three-dimensional data was extracted and a surface was constructed. Each surface is introduced into a discretized channel such that it is located in the center of the channel (on the x–y plane). The channel maintains the aspect ratio and boundary conditions of the *in vitro* experiments. The inlet condition is defined by steady rectilinear flow within a rectangular channel.[11] The channel walls and platelet aggregation surface have a no slip condition imposed. A Neumann velocity condition is imposed on the outlet. The OpenFOAM solver package was used to solve the incompressible Newtonian Navier–Stokes equations.[10] The equations were solved to steady state using the SIMPLE algorithm[17] over a polyhedral finite volume spatial discretization. The local shear rate is defined such that:

$$|\gamma_{Local}| = 2\sqrt{J_2} \tag{6}$$

where J_2 is the second invariant of the rate of strain tensor.[3]

RESULTS

The present technique offers the ability to measure platelet aggregation geometries developing in response to known upstream shear rates and exposure times. Experiments were conducted using two methodologies: first platelet aggregations were grown at three different upstream shear rates (1200, 1600, and 1800 s^{-1}) using a very long exposure time (10 min) allowing the effect of shear rate on the geometry of mature platelet aggregations (no longer growing) to be studied. The second set of experiments was conducted at a constant upstream shear rate (1800 s^{-1}) using a range of exposure times (1.5–10 min) to study the geometries of growing platelet aggregations.

The number of platelet aggregations available for analysis depended on the density of platelet aggregations (platelet aggregations per unit area) forming inside the microchannel, which was observed to be a function of both upstream shear rate and exposure time. The numbers of mature platelet aggregations analyzed were: 20, 31, and 34 platelet aggregations at shear rates 1200, 1600, and 1800 s^{-1}. For the experiments with varying exposure times 2, 4, 15, 20, 25, 23, 26, and 28 platelet aggregations were measured for exposure times of 1.5, 2.0, 2.5, 3.0, 4.0, 5.0, 6.0, and 10 min, respectively.

Effect of Shear Rate on Mature Platelet Aggregation Geometries

Figure 3 shows the correlation between mature platelet aggregation height, represented by the average centroid height, z_c (Eq. 2), and the upstream shear rate. As the upstream shear rate increases from 1200 to 1800 s^{-1}, there is an approximately linear increase in mature platelet aggregation height. If the linear trend is assumed to persist at lower shear rates then the minimum required upstream shear rate for platelet

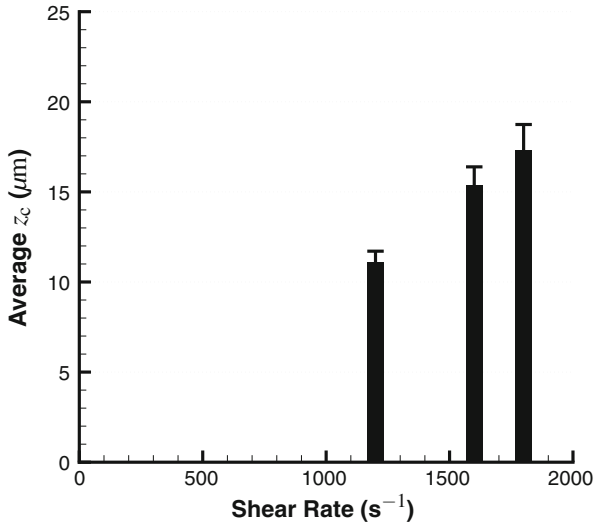

FIGURE 3. Average centroid height (z_c) of mature platelet aggregations (exposure time 10 min) as a function of upstream shear rates. *Error bars* represent standard error (Student's *t* test; $p = 0.10$) from 20, 31, and 34 independent platelet aggregations at $\gamma_{Pw} = 1200$, 1600, and 1800 s^{-1}, respectively.

aggregation can be inferred to be approximately 140 s^{-1} (137.143 ± 0.085 s^{-1}). However, further investigations are required to determine precisely this threshold. It was also observed that the density of platelet aggregations forming on the microchannel surface was larger at higher shear rates (data not shown).

To further investigate the effect of upstream shear rate on platelet aggregation shapes, the location of the in-plane centroid at different heights, or z levels, within a platelet aggregations were calculated. The effect of increasing the upstream shear rate on normalized centroid locations, x_c^* and y_c^* (Eq. 5) at three different shear rates is shown in Fig. 4. At an upstream shear rate of 1200 s^{-1} the average platelet aggregation geometries is essentially symmetrical with both x_c^* and y_c^* approximately equal to zero for all heights.

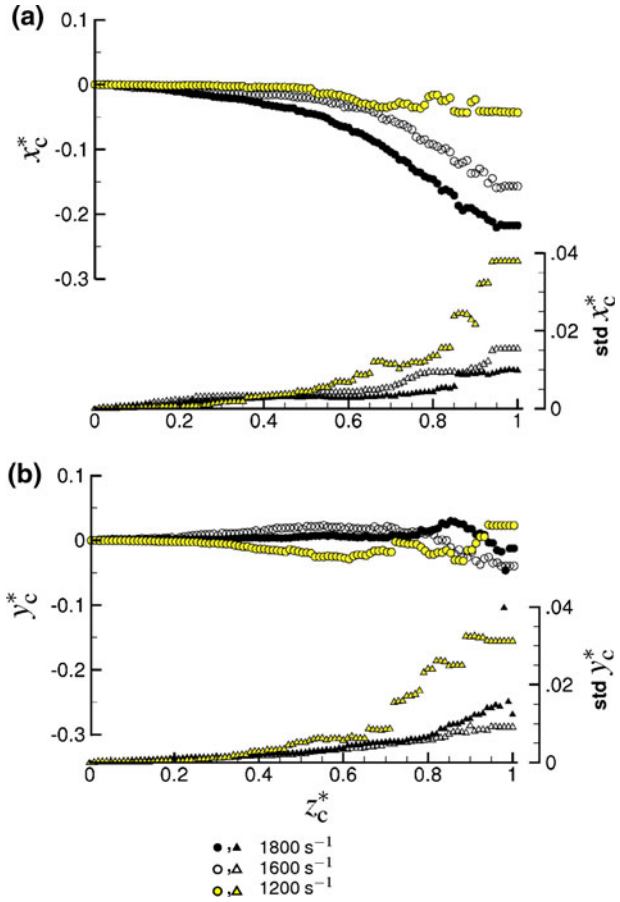

FIGURE 4. Variation of normalized centroid length and width (x_c^* and y_c^*) with platelet aggregation height at three different upstream shear rates. (a) x_c^* is approximately constant at γ_{Pw} = 1200 s^{-1} but at γ_{Pw} = 1600 and 1800 s^{-1} x_c^* moves towards upstream at higher z levels indicating that the platelet aggregation apex is forward of center. (b) y_c^* remains approximately constant at all shear rates indicating that on average the platelet aggregations are symmetrical with respect to the x axis. The standard error of x_c^* and y_c^* are shown in the lower portion of (a) and (b), respectively.

However, as the upstream shear rate increases further, the average platelet aggregation geometries becomes increasingly asymmetric in the streamwise direction, with x_c^* becoming significantly less than zero. The decrease in x_c^* at high z^* indicates that the platelet aggregation centroid is moving upstream. The normalized centroid width is nearly constant for all shear rates (Fig. 4b) indicating that there was no preference for the platelet aggregations to develop towards either channel wall.

Averaged Three-Dimensional Platelet Aggregations at Different Shear Rates

Averaged mature platelet aggregation geometries at each shear rate were developed using an elliptical fitting method and Eq. (4). While the average platelet aggregation geometries do not physically model individual platelet aggregations, they show very clear changes between data sets: in this case as upstream shear rate is varied. The three-dimensional profiles for the average platelet aggregations at each shear rate are illustrated in Fig. 5. As the upstream shear rate increases from 1200 to 1800 s^{-1} the platelet aggregation apex moves upstream. This is consistent with the decrease in x_c^* at higher z* values seen in Fig. 4. At an upstream shear rate of 1200 s^{-1} the cross-sectional area is approximately constant and centered about the base centroid up to 40% of the maximum height. Above this height the platelet aggregation exhibits a pyramid-like tapering with a rapid decrease in cross-section and only a very slight upstream movement in the in-plane position of the centroid with increasing height. The average geometries at 1600 and 1800 s^{-1} are quite different: within the platelet aggregations with increasing height there is a clear movement of the in-plane centroid upstream and the upstream bias is greater at the higher shear rate. This causes the front or upstream surface of the platelet aggregations to be relatively steep while downstream of the platelet aggregation apexes the surface height decreases more gradually. As expected at all shear rates the average platelet aggregation geometries is symmetric in the cross-stream direction. In addition, the volume of the average thrombus increases with increasing shear rate with volumes of 1.3675 × 10^5, 2.02 × 10^5, and 2.2945 × 10^5 μm^3 at shear rates of 1200, 1600, and 1800 s^{-1}, respectively. This trend can be inferred from Figs. 3 and 5.

The shapes of the ellipses forming the averaged platelet aggregation geometries at each z level in Fig. 5 appear remarkably uniform, with successive levels lying on top of and inside underlying layers. To confirm this observation and compare between upstream shear rates, the platelet aggregation geometry ratio,

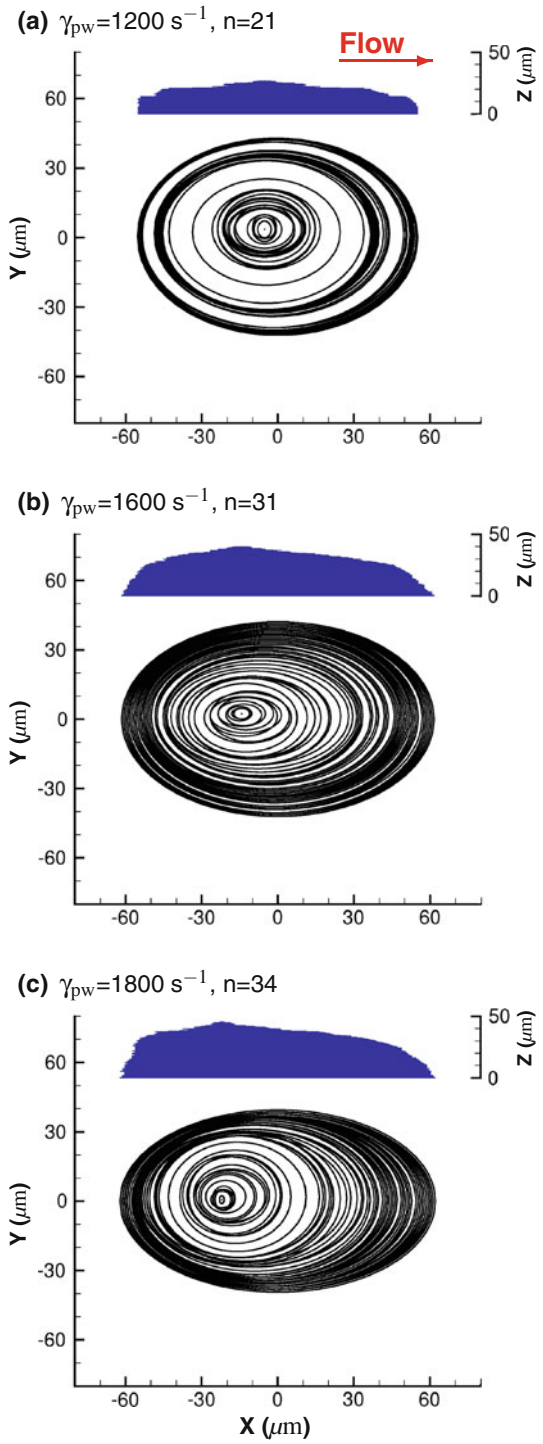

FIGURE 5. Average mature platelet aggregation geometries at (a) γ_{Pw} = 1200 s^{-1}, (b) γ_{Pw} = 1600 s^{-1}, and (c) γ_{Pw} = 1800 s^{-1} calculated by least squares fitting of an ellipse at each *z* level, with Δz = 1 μm.

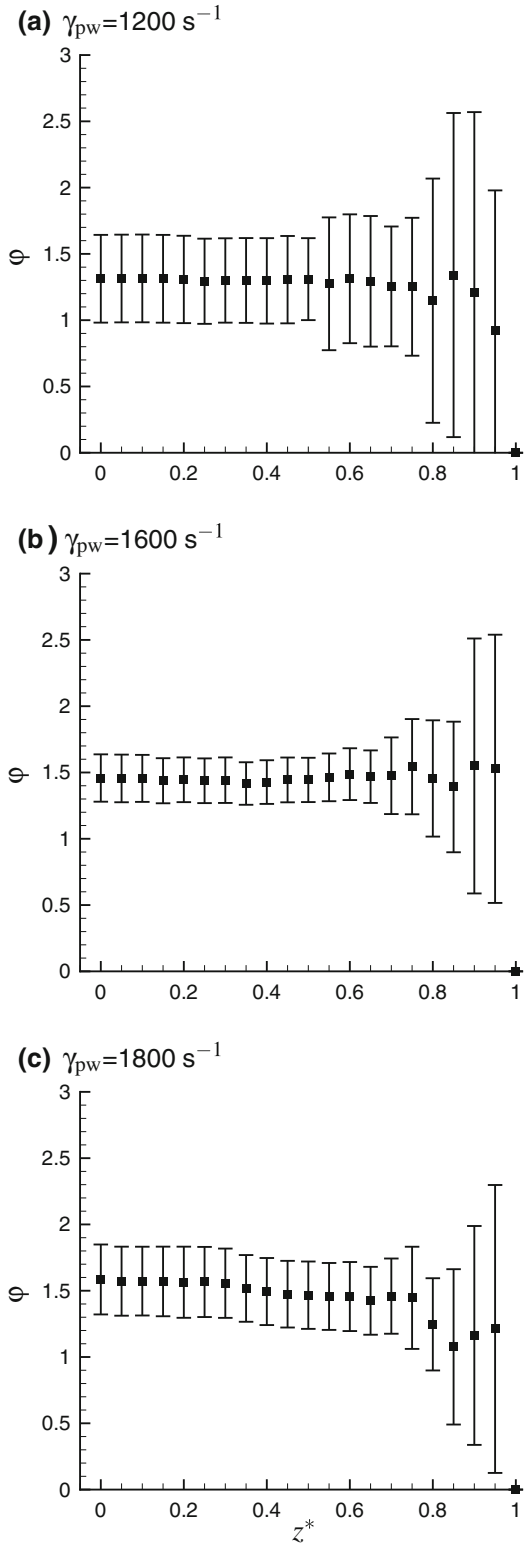

FIGURE 6. Variation of normalized geometry ratio φ of fitted ellipse with normalized platelet aggregation height at (a) γ_{Pw} = 1200 s^{-1}, (b) γ_{Pw} = 1600 s^{-1}, and (c) γ_{Pw} = 1800 s^{-1}. The ratio is nearly constant for all shear rates. *Error bars* represent Student's *t* test from 20, 31, and 34 independent platelet aggregations (p = 0.10) at γ_{Pw} = 1200, 1600, and 1800 s^{-1}, respectively.

defined as $\varphi = a^*_{avg}/b^*_{avg}$, is plotted in Fig. 6 for all shear rates. The standard error of the geometry ratio increases above 80% of maximum height due to increased variability and roughness at the platelet

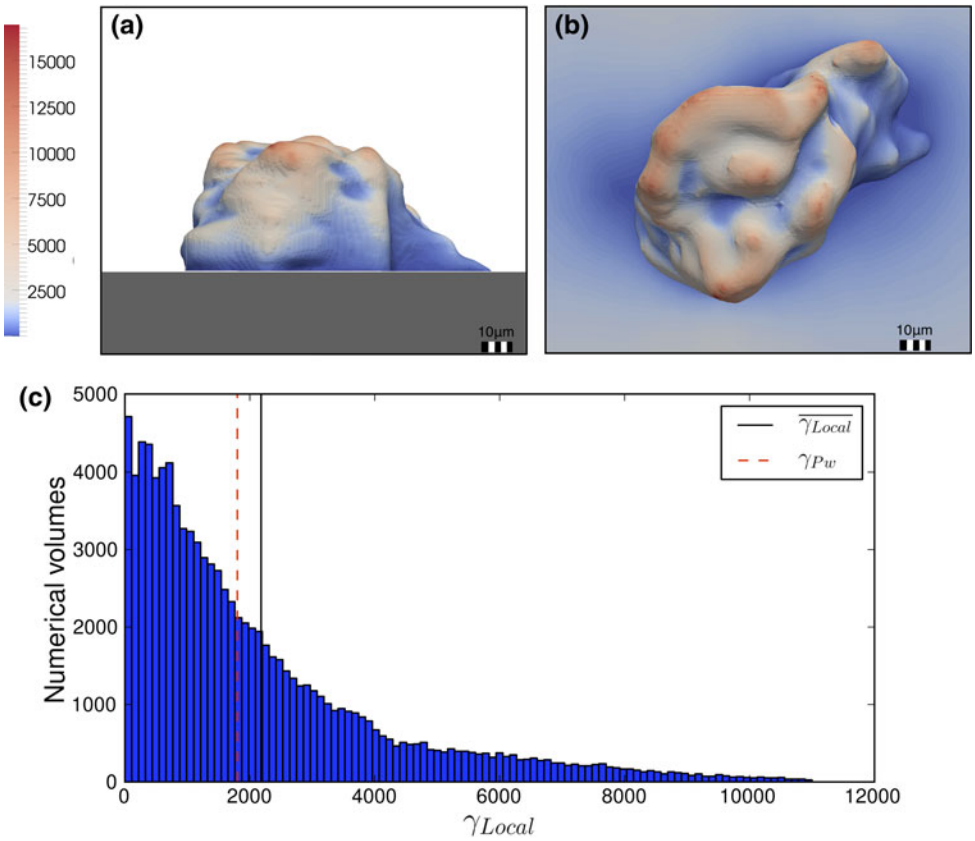

FIGURE 7. Local shear rate distribution (γ_{Local}) around a representative mature platelet aggregation at $\gamma_{Pw} = 1800\ s^{-1}$. *The side view* (a) and *top view* (b) show local shear rates lower than γ_{Pw} in *blue shades* and local shear rates higher than γ_{Pw} in *red shades*. In both (a) and (b) the flow is from *left* to *right*. The highest local shear rates, up to eight times greater than γ_{Pw} occur on the upper surfaces of the platelet aggregations while low shear regions occur on the adjacent walls, the lower surfaces of the platelet aggregations and the region at the very rear of the platelet aggregations. A histogram of γ_{Local} on the platelet aggregation surface is shown in (c). The average value of γ_{Local} indicated by the *solid black line* is 21% greater than the upstream wall shear rate ($\gamma_{Pw} = 1800\ s^{-1}$) indicated by the *dashed red line*.

aggregation surface. Averaging over all shear rates, and excluding data above 80% of the maximum height, the geometry ratio of the mature platelet aggregations is 1.42 ± 0.29. The approximately constant geometry ratio indicates that the average cross-sectional geometry of the mature platelet aggregations is independent of upstream shear rate and height.

Distribution of Local Shear Around a Platelet Aggregation

The distribution of local shear rate on the surface of a mature platelet aggregation, generated by numerically simulating the flow, is shown in Figs. 7a and 7b. The geometry was digitized from a platelet aggregation generated by blood flow experiments at $\gamma_{Pw} = 1800\ s^{-1}$ and the simulations were run at the same upstream wall shear rate. Regions of local shear rate that are higher than the upstream wall shear rate ($\gamma_{Local} > \gamma_{Pw}$) are shaded red, with these higher shear rates occurring on the upper surfaces of the platelet aggregations. The peak local shear rates are approximately eight times greater than the upstream wall shear rate and coincide with regions of the platelet aggregation that are both sharply curved and exposed to the oncoming flow. Regions of low shear rate ($\gamma_{Local} < \gamma_{Pw}$) are shaded blue, and are found on the lower regions of the platelet aggregation as well as in sheltered concave pockets elsewhere on the surface. In Fig. 7b the blue region on the channel wall surrounding the platelet aggregation shows that the platelet aggregation also invokes low channel wall shear rate, particularly upstream and downstream. Significantly, Figs. 7a and 7b shows a low shear region on the downstream face of the platelet aggregation and the adjacent floor of the microchannel. The general features described above for the mature platelet aggregations in Fig. 7 were also observed in all four additional simulations of other mature platelet aggregations at $\gamma_{Pw} = 1800\ s^{-1}$.

The values of local shear rate on the platelet aggregation surface were analyzed to generate the histogram shown in Fig. 7c, where the vertical axis

represents the number of computational volumes. The histogram clearly demonstrates that the local shear rate on the surface of the platelet aggregation differs significantly from the upstream shear rate. The high histogram values for low local shear rate ($\gamma_{Local} < \gamma_{Pw}$) indicate that a significant portion of the platelet aggregation surface experiences very low shear rate, however, the average shear rate on the surface (of $\gamma_{Local} = 2179\ s^{-1}$) is 21% greater than γ_{Pw}.

Geometries of Growing Platelet Aggregations ($\gamma_{Pw} = 1800\ s^{-1}$)

In the second part of the experiment, the time history of platelet aggregation growth was studied at an upstream shear rate of 1800 s^{-1} by allowing platelets to aggregate for exposure times ranging from 1.5 to 10 min. The blood used in this experiment was from a different donor so the platelet aggregation heights may vary slightly from those presented in the previous sections. The average platelet aggregation centroid height at different exposure times is presented in Fig. 8a. At the lowest exposure times (1.5 and 2 min) only a few monolayer platelet aggregations are observed and the number of aggregations was too low for statistical significance. At exposure times beyond 2.5 min a significant number of platelet aggregations were observed with centroid height increasing steeply with exposure time before levelling off after 5 min.

At each exposure time, averaged platelet aggregation geometries were calculated using the method described earlier. In mature platelet aggregations, the geometry ratios were relatively constant throughout the height of platelet aggregations at a given exposure time. However, there was a systematic change in the geometry ratio with increasing exposure time: the geometry ratio averaged over the platelet aggregation height (φ_{ave}) increases as the platelet aggregation matures, as shown in Fig. 8b. Note, φ_{ave} was calculated between the platelet aggregation base and 80% of maximum height as the upper surface of the platelet aggregation is not smooth, generating significant errors in the fitting process. The average geometry ratio grows gradually with increasing exposure time; from $\varphi_{ave} = 1.2 \pm 0.15$ at 2.5 min to $\varphi_{ave} = 1.49 \pm 0.06$ at 10 min indicating that on average in the early stages of development the platelet aggregations are almost circular, becoming more elongated in the flow direction as they mature.

Figure 8c shows a z–x cross-section through the center of the average platelet aggregation geometries at different exposure times. As demonstrated in Fig. 8d once initial platelet recruitment begins, the majority of subsequent recruitment occurs at or downstream of the original recruitment site. Thus the platelet aggregation geometries in Fig. 8c are plotted with their most upstream point as $x = 0$. The cross-section area, platelet aggregation height, and length all increase with increasing exposure time. It is noticeable that the platelet aggregation length is growing more rapidly than the height, while from Fig. 8b we also know that the platelet aggregation length also grows faster than its width. Thus the statistical data for the averaged platelet aggregations presented in Figs. 8a to 8c is consistent with the representative aggregation sequence shown in Fig. 8d.

CONCLUSIONS

A combination of *in vitro* and numerical experiments has provided insight into the shear rate dependence of platelet aggregation geometries. Even within the relatively narrow range of upstream shear rates examined, 1200 $s^{-1} < \gamma_{Pw} < 1800\ s^{-1}$, significant and systematic variations in average platelet aggregation geometries were found. Increases in γ_{Pw} generated not only taller platelet aggregations but also caused changes in platelet aggregation geometry, with a greater tendency for the apex of the platelet aggregation to move forwards generating a more elongated rear platelet aggregation surface. Remarkably, the average aspect ratio of each z slice of the mature platelet aggregation geometries was constant throughout the platelet aggregation height at $\varphi = 1.42 \pm 0.29$, and did not vary with upstream shear rate.

The local shear rate on the surface of a platelet aggregation was shown to be significantly different from the upstream shear rate. The peak local shear rate over a mature platelet aggregation (at $\gamma_{Pw} = 1800\ s^{-1}$) was over 800% greater than γ_{Pw} while the mean local shear rate was 21% greater than γ_{Pw}. Whilst upstream shear rate is clearly an important parameter it is a poor measure of the shear rate that a platelet experiences as it travels over, and adheres to, an existing platelet aggregation. Previous investigation[8] has shown that the sequence of shear rate experienced by a platelet moving over a platelet aggregation is a critical factor in platelet aggregation. However, this is the first time that the very extensive variation in shear rate over a platelet aggregation surface has been quantified.

Experiments on growing platelet aggregations revealed significant changes in shape as the platelet aggregations matured, with smaller platelet aggregations being almost circular in shape, and becoming more elongated as they mature. This change in shape is consistent with the observation that platelets preferentially adhere toward the rear of growing platelet aggregations but also has implications for how a platelet aggregation stops growing. The local flow field

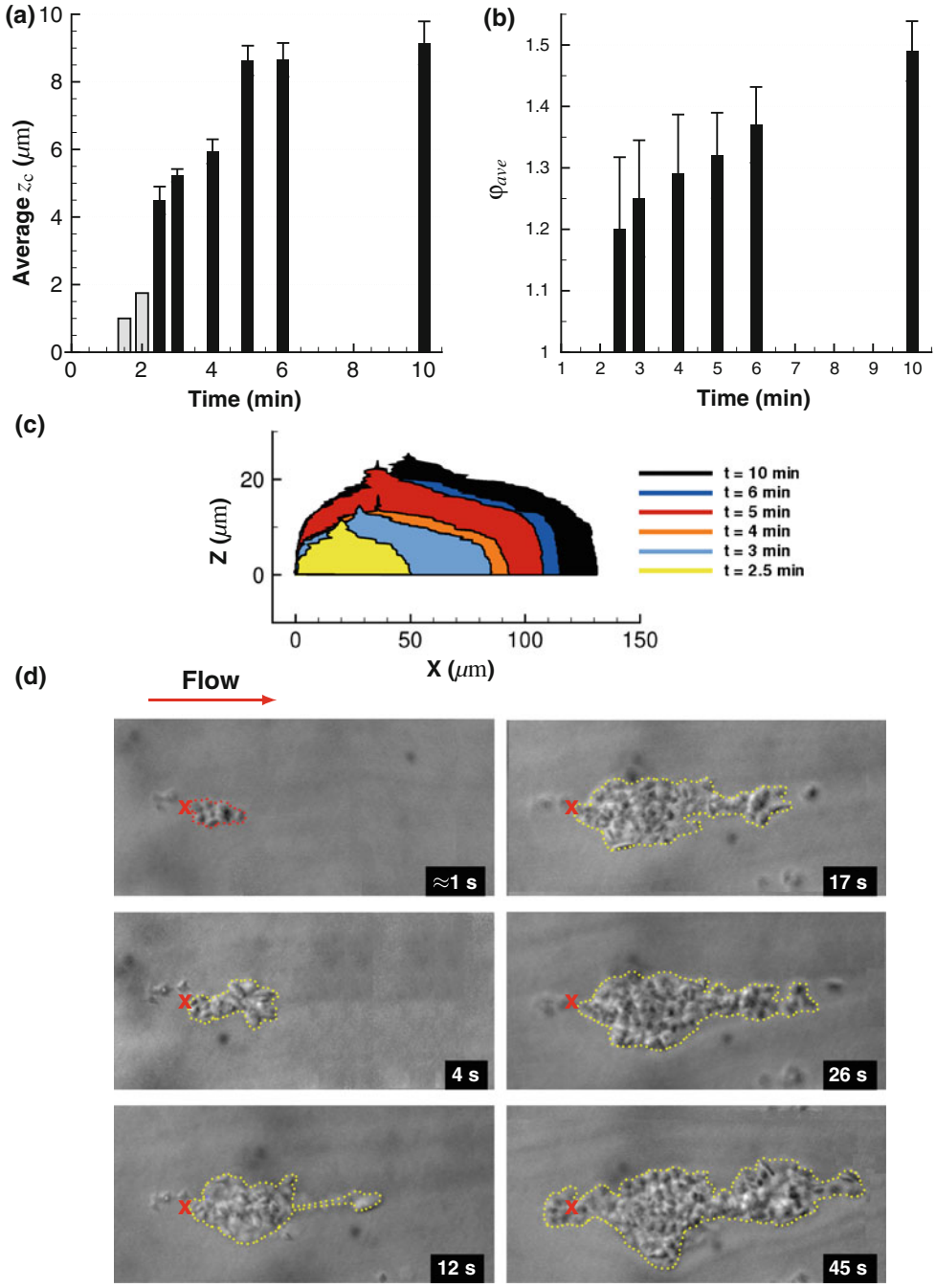

FIGURE 8. Platelet aggregation development at γ_{Pw} = 1800 s^{-1}. (a) Average centroid height (z_c). The first two *grey columns* demonstrate the centroid height of the monolayer platelet aggregations. The *solid black columns* show the average height calculated from between 15 to 28 platelet aggregations, with *error bars* represent Student's *t* test (p = 0.10). (b) Normalized geometry ratio showing a change in average platelet aggregation shape from nearly circular to elliptical as platelet aggregations develop, *error bars* represent Student's *t* test (p = 0.10). (c) Variation of average cross-sectional area with exposure time. (d) Bright field images showing the time-lapsed development of a platelet aggregation. The initial aggregation at t = 1 s consists of approximately seven platelets indicated by the *broken red line*. The majority of subsequent recruitment, *broken yellow line*, occurs downstream of the initial aggregation point marked by a *red cross*.

around a platelet aggregation is complex and highly geometry dependent. Thus systematic changes in the geometry of growing platelet aggregations infer systematic changes in the shear rate path experienced by platelets adhering to these platelet aggregations. A corollary, yet to be proven, is that the mature platelet aggregation geometries generate shear rate paths that suppress further platelet aggregation.

ACKNOWLEDGMENTS

The authors gratefully acknowledge access to the facilities of the Australian Centre for Blood Disease (ACBD) and support from the ARC under Discovery grant DP0987643.

REFERENCES

[1]Bhatt, D. L., and E. J. Topol. Scientific and therapeutic advances in antiplatelet therapy. *Nat. Rev.* 15:15–28, 2003.
[2]Fouras, A., D. Lo Jacono, C. V. Nguyen, and K. Hourigan. Volumetric correlation PIV: a new technique for 3D velocity vector field measurement. *Exp. Fluids* 47:569–577, 2009.
[3]Fung, Y. Biomechanics: Mechanical Properties of Living Tissues. New York: Springer, 1993.
[4]Huo, Y. Q., and K. F. Ley. Role of platelets in the development of atherosclerosis. *Trends Cardiovasc. Med.* 14:18–22, 2004.
[5]Jackson, S. P. The growing complexity of platelet aggregation. *Blood* 109:5087–5095, 2007.
[6]Mangin, P., C. L. Yap, C. Nonne, S. A. Sturgeon, I. Goncalves, Y. P. Yuan, S. M. Schoenwaelder, C. E. Wright, F. Lanza, and S. P. Jackson. Thrombin overcomes the thrombosis defect associated with platelet gpvi/fcr gamma deficiency. *Blood* 107:4346–4353, 2006.
[7]Maxwell, M. J., E. Westein, W. S. Nesbitt, S. Giuliano, S. M. Dopheide, and S. P. Jackson. Identification of a 2-stage platelet aggregation process mediating shear-dependent thrombus formation. *Blood* 109:566–576, 2007.
[8]Nesbitt, W. S., E. Westein, F. J. Tovar-Lopez, E. Tolouei, A. Mitchell, J. Fu, J. Carberry, A. Fouras, and S. P. Jackson. A shear gradient-dependent platelet aggregation mechanism drives thrombus formation. *Nat. Med.* 15: 665–673, 2009.
[9]Ono, A., E. Westein, S. Hsiao, W. S. Nesbitt, J. R. Hamilton, S. M. Schoenwaelder, and S. P. Jackson. Identification of a fibrin-independent platelet contractile mechanism regulating primary hemostasis and thrombus growth. *Blood* 112:90–99, 2008.
[10]OpenCFD Limited 2010, OpenCFD Limited, Reading. http://www.openfoam.com. Accessed 22 Nov 2010.
[11]Papanastasiou, T., G. Georgiou, and A. Alexandrou. Viscous Fluid Flow. Boca Raton: CRC, 2000.
[12]Ross, R., and J. A. Glomset. Pathogenesis of atherosclerosis. *N. Engl. J. Med.* 295:369–377, 1976.
[13]Ruggeri, Z. M. Platelets in atherothrombosis. *Nat. Med.* 8:1227–1234, 2002.
[14]Ruggeri, Z. M. The role of von willebrand factor in thrombus formation. *Thromb. Res.* 120:S5–S9, 2007.
[15]Ruggeri, Z. M., and G. L. Mendolicchio. Adhesion mechanisms in platelet function. *Circ. Res.* 100:1673–1685, 2007.
[16]Savage, B., F. Almus-Jacobs, and Z. M. Ruggeri. Specific synergy of multiple substrate–receptor interactions in platelet thrombus formation under flow. *Cell* 94:657–666, 1998.
[17]Versteeg, H. K., and W. Malalaekera. Computational Fluid Dynamics. London: Longman Group, 1995.